Probing molecular layers with low-energy electrons

Tebyani, A.

3

Comparison of Pentacene Layer Growth on Graphite and hBN Flakes *

Abstract

We use PhotoElectron Emission Microscopy (PEEM) and Low-Energy Electron Microscopy (LEEM) to study the growth dynamics of pentacene layers on graphite and hexagonal boron nitride (hBN) flakes in real-time. These two substrates have similar atomic surface lattices but different electronic band structures. On both substrates, we find pentacene molecules to initially cover the flake surface with a flat-lying wetting layer. From diffraction and dark-field images, we find the wetting layer to be comprised of crystalline domains in six different orientations. Subsequently, pentacene layer growth proceeds in notably different manners on the two substrates, forming tilted recumbent crystalline domains on graphite versus standing-up thin film phase crystals on hBN. We discuss these results in light of the multi-faceted way in which different factors such as the electronic density of states of the surface, templating due to surface lattice structure, and cleanliness of the surface affect the growth of the molecular adlayer. We also measure LEEM reflectivity spectra related to the unoccupied density of states above the vacuum level, of the wetting layer on both substrates. We argue that the stronger electronic interaction between pentacene and graphite, compared to hBN, is responsible for the difference between the LEEM reflectivity spectra as well as the formation of different pentacene phases growing on the two substrates after the wetting layer has formed.

---

* This chapter has been submitted for publication as “Comparison of Pentacene Layer Growth on Graphite and hBN Flakes”, A. Tebyani, R.M. Tromp, S.J. van der Molen

3.1 Introduction

Van der Waals (vdW) materials have emerged in recent years as a promising class of substrate materials for growth of molecular layers. One approach is to combine molecular adlayers with vdW materials to create heterostructures with tailored new properties. For instance, p-n heterojunctions stemming from the combination of pentacene and MoS_2 are found to be gate-tunable and exhibit interesting photovoltaic effects, such as ultrafast (several picoseconds) charge transfer and a long-lived charge-separated state. [1,2] Other examples include gate-tunable vertical graphene-pentacene barristor devices [3] or doping effects caused in graphene by adsorbate NO_2 molecules. [4] Another approach is to use vdW materials as substrates for growth of molecular layers on top, allowing for investigation of properties such as charge transport in molecular crystals near the monolayer limit. Some examples include devices made with few-layer crystalline pentacene on hBN [5], few-layer dioctylbenzothienobenzothiophene molecular crystals on graphene and boron nitride [6] and films of rubrene on hBN [7]. The underlying vdW material can also alter the growth of the molecular layer on top, potentially creating new phases.

In this chapter, we use pentacene as a model aromatic organic molecule. Over the years, pentacene has been the subject of intense study due to its excellent properties such as high charge carrier mobility of above 1 $cm^2V^{-1}s^{-1}$ in both single crystal and thin film devices. [5,8–11] Since the first real-time observations of pentacene growth on silicon and organically-terminated silicon [12], the growth and structure of pentacene layers on various other substrates such as SiO_2, Al_2O_3, Au(111), Ag(110), Ag(111), Cu(110) and Bi(001), among others, have been the subject of many studies. [13–22] More recently, pentacene growth on vdW materials is also being investigated, with promising results. [1,2,5] Here, we study the growth of pentacene layers on two basic vdW systems, i.e. graphite and bulk hexagonal boron nitride (hBN). Graphite is a conductor, chemically rather inert with a hexagonal surface lattice closely matching the aromatic ring structure of pentacene. hBN also has a hexagonal lattice, with similar unit cell parameters to graphite. However, in contrast to graphite, hBN is an insulator, making it a useful substrate for transport studies of molecular adlayers. [5] There have been a few reports of pentacene layer growth on hBN flakes so far. [5,23–25] However, these show discrepancies regarding the structure of the pentacene layers.

We use Low-Energy Electron Microscopy (LEEM) to study the growth of pentacene layers on exfoliated graphite and hBN flakes. We observe the growth dynamics of the pentacene layers in real-time using PhotoElectron Emission Microscopy (PEEM). Furthermore, we probe the local microstructure of the layers, in real-space and diffraction-space, using Low Energy Electron Microscopy (LEEM). We also measure LEEM reflectivity spectra, which

are directly related to the unoccupied density of states (DOS) above the vacuum level, of the pentacene layers on top of the two substrates. We analyze the similarities and the differences in the resulting pentacene layers, and discuss the results in terms of the factors affecting layer growth such as the templating effect from the substrate, electronic band structure of the substrate and surface cleanliness.

3.2 Experimental Technique

In the LEEM instrument, electrons are emitted from an electron gun with a kinetic energy of 15 keV. [26,27] Before reaching the sample, an electric field of ~10 kV/mm between an objective lens and the sample (spaced at 1.5 mm) decelerates the electrons to an energy of just a few eV. This interaction energy can be precisely tuned by changing the sample potential with respect to the grounded objective lens. After interaction with the sample, the reflected electrons are re-accelerated by the same electric field and guided toward the detector screen, also passing through an aberration-correcting path along the way. On the detector, a real-space or a diffraction image can be displayed. Furthermore, illumination with a Hg discharge lamp allows for PEEM with UV photons. The photoelectrons are collected in the same way as the reflected electrons from the electron gun. A Knudsen cell evaporator is attached to the sample chamber with line of sight to the substrate surface, allowing for *in situ* pentacene sublimation and growth.

Graphite and hBN flakes were exfoliated onto silicon substrates (with native oxide) with the Scotch tape method. Typical thicknesses of the flakes are several tens of nanometers. Prior to the growth experiments, the samples were heated to ~500˚C overnight in the UHV chamber of LEEM (~1×10^{-9} mbar) in order to clean the flake surfaces. Growth and characterization of the samples were carried out in ultrahigh vacuum (UHV) and at room temperature, unless stated otherwise.

3.3 Results

Pentacene on Graphite:

Figs. 3.1(a) and (b) show PEEM images of a graphite flake prior to and after a period of pentacene sublimation, respectively. On the SiO_2 substrate surrounding the graphite flake, many bright nucleation spots have appeared in Fig. 3.1(b). These areas indicate growth of pentacene in standing-up thin film phase with a herringbone crystal structure (see Fig. 1.1 in

chapter 1), which proceeds in the same manner as already reported in the literature for growth of pentacene on flash-cleaned silicon or SiO_2. [12,17] The graphite flake remains dark in PEEM compared to the substrate, however the photoemission intensity on the flake as a whole shows a gradual increase as pentacene is deposited (see Fig. 3.1(g)). The elliptical spot in Fig. 3.1(b) is due to an electron beam imprint after LEEM imaging. Figs. 3.1(c-f) show the developments on the area of the graphite flake indicated by the dashed rectangle in Fig. 3.1(b) during the pentacene sublimation process. The contrast has been readjusted to better reveal the changes. We observe regions of lower intensity gradually growing from the edges of the flake. We will refer to these darker areas as phase A and the rest of the flake as phase B.

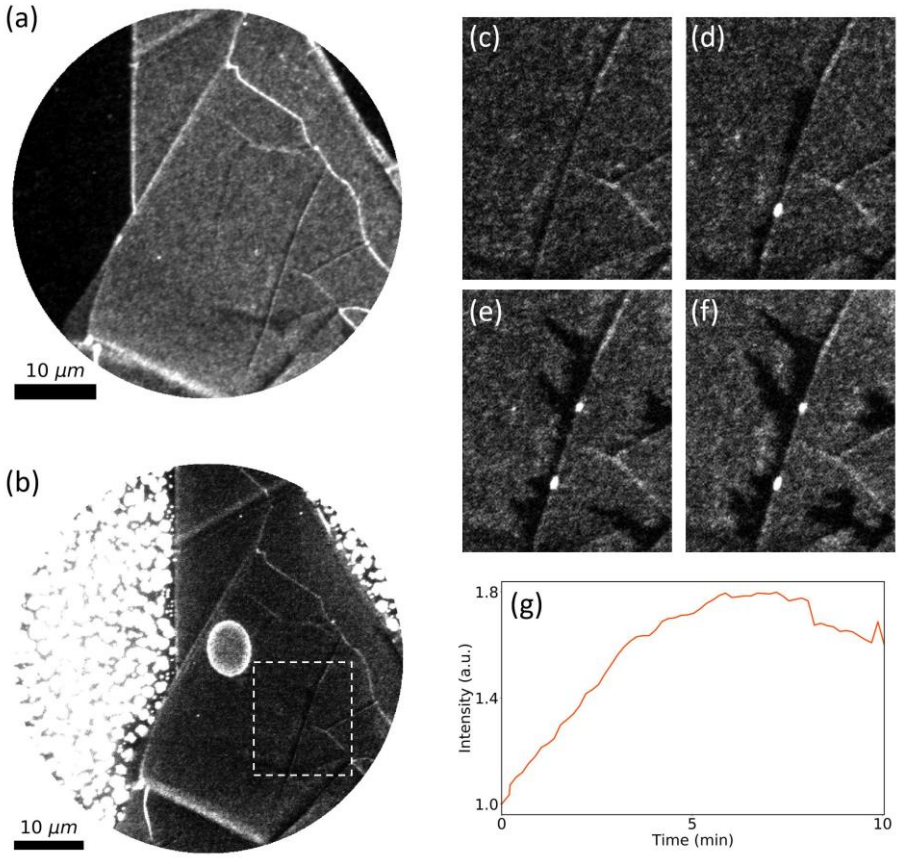

Fig. 3.1 PEEM images of pentacene growth on a graphite flake (grey) on SiO_2 (black) (a) before the start of pentacene sublimation. (b) some time after the start of sublimation. The contrast has been re-adjusted. The elliptical spot is due to beam imprint. (c-f) contrast-readjusted sequence following the changes during sublimation in PEEM images on the area marked with a rectangle in (b). The dark regions in these images are referred to in the text as phase A, and the rest of the flake as phase B. (g) increase in photoemission intensity during the initial stage of sublimation

To investigate the structure of the two different regions on the graphite flake, i.e. phases A and B, we employ the electron beam. Fig. 3.2(a) shows a bright-field LEEM image of an area on the graphite flake, containing both phases. To obtain such an image, an aperture is placed in a diffraction plane to only transmit the 0^{th}-order diffraction spot. Phase A appears as the bright region at the bottom of Fig. 3.2(a) and has the diffraction pattern shown in Fig. 3.2(b). Phase B forms stripe patterns on the rest of the surface of the flake and corresponds to the diffraction pattern in Fig. 3.2(c). To further investigate phase B, we placed apertures on each of the twelve diffraction spots so as to obtain dark-field images. The dark-field images for six of the diffraction spots (numbers 1, 2, 5, 6, 9, 10 in Fig. 3.3(a)) are displayed in Fig. 3.3(d-i). Here, the bright areas only show those pentacene regions that have the crystal orientation chosen. The dark-field images in Fig. 3.3(d-i) and their superimposition in Fig. 3.3(c) reveal that pentacene forms stripe-shaped crystals that appear dark in the corresponding bright-field image of the same area, see Fig. 3.3(b) (and similarly Fig. 3.2(a)). Due to symmetry, dark-field images corresponding to the other diffraction spots (3, 4, 7, 8, 11, 12 as annotated in Fig. 3.3(a)), light up exactly the same areas as those shown in Fig. 3.3(d-i). Hence, pentacene in phase B forms long narrow crystals in six different azimuthal orientations on the surface of the flake. These orientations can be grouped into three pairs, with a rotation of 120˚ between different pairs and a smaller splitting angle between the diffraction points of each pair. Such pairs in Fig. 3.3(a) are the spots 1-2, 5-6, and 9-10. Interestingly, the domains associated with each pair are also located spatially close to one another, see Figs. 3.3(d-g), (e-h), (f-i).

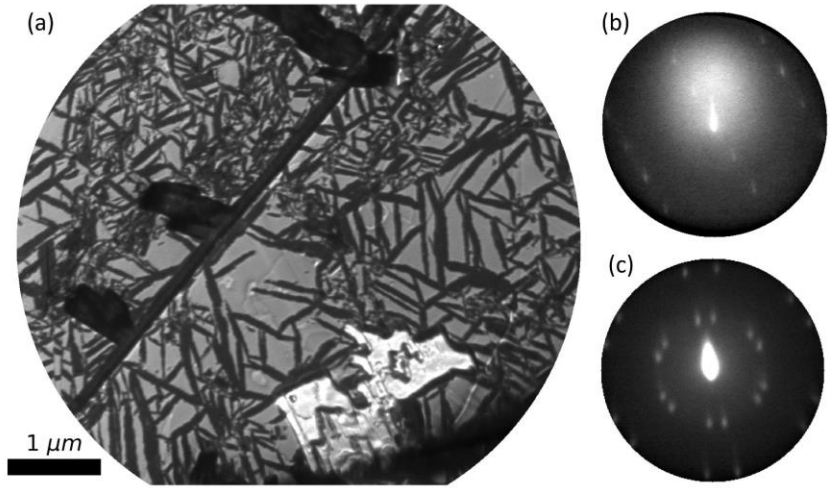

Fig. 3.2 LEEM images of pentacene on graphite. (a) bright-field image of an area containing two different pentacene phases: A (bright at the bottom) and B (the stripe patterns) (b) diffraction pattern corresponding to phase A. (c) diffraction pattern corresponding to phase B.

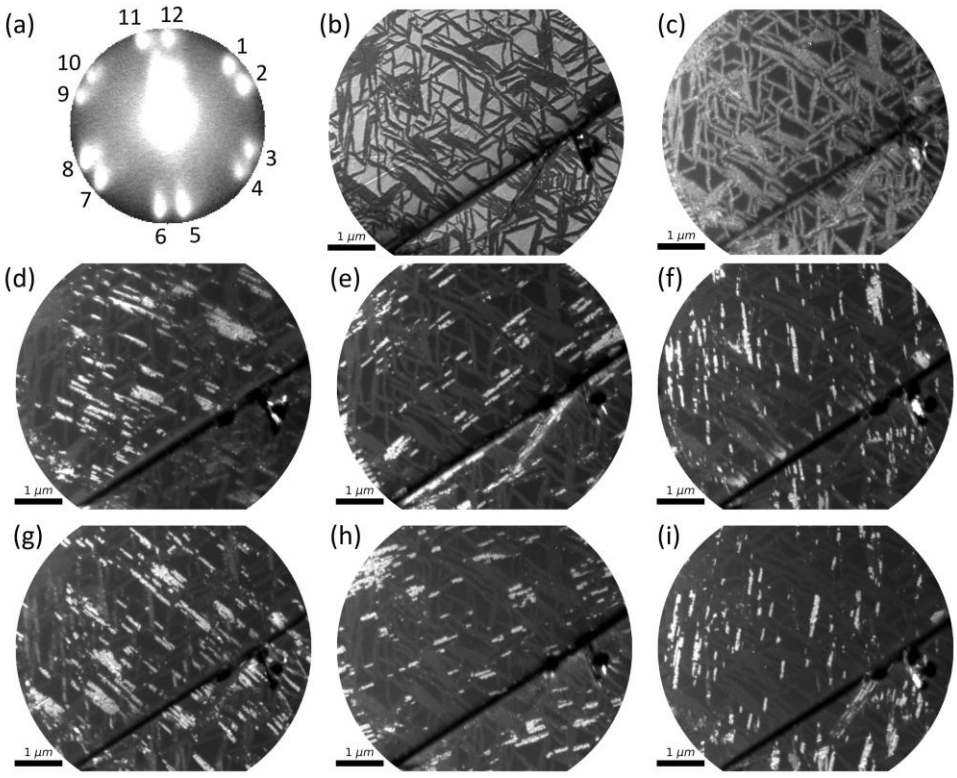

Fig. 3.3 Bright-field and dark-field images of pentacene phase B on graphite. (a) annotation of diffraction spots for dark-field images (b) bright-field image (c) all six dark-field images in (d-i) superimposed. Pentacene areas are bright and create the same pattern as the dark areas in the bright-field image (d-i) dark field images corresponding to diffraction spots 1, 2, 5, 6, 9, 10 with the following correspondence: 1:d, 2:g, 5:e, 6:h, 9:f, 10:i. Areas corresponding to each pair of adjacent diffraction peaks (i.e., 1-2, 5-6, 9-10) are located spatially close to one another. The beam energy used for imaging (e), (d) and (h) is 0.5 eV, while it is 0.6 eV for (b), (f), (g) and (i).

Pentacene on hBN:

Next, we present the dynamics of growth of pentacene layers on top of hBN flakes imaged in real-time with PEEM. In several cases we could also obtain diffraction patterns of the pentacene crystals using the electron beam. Still, the insulating nature of hBN poses challenges towards full characterization with an electron beam.

The initial stage of growth of pentacene on hBN flakes proceeds in a similar fashion to the growth of pentacene layers on graphite. Initially, bright nucleation spots (in PEEM images) appear on the SiO_2 substrate indicating standing-up thin film phase growth. The hBN flake itself remains relatively dark, although it shows some gradual increase in photoemission

intensity (see Fig. 3.4(d)). Shining the electron beam on the flakes at this stage reveals a diffraction pattern, indicating adsorption and organization of pentacene on the hBN flake surface. We will refer to this pentacene phase as phase C, with the corresponding diffraction pattern shown in Fig. 3.5(a). Note that Fig. 3.5(a) is very similar to Fig. 3.2(c), i.e. phase B on graphite. Fig. 3.5(a) is obtained by a higher-energy incoming electron beam (20.6 eV), and hence, reveals more of the diffraction pattern compared to Fig. 3.2(c) (obtained by a beam of 2.5 eV electrons). With continued sublimation, what we typically observe in PEEM is the emergence of bright spots on the flakes (with similar intensity to the nucleation spots on SiO_2). These nucleation spots gradually grow until they cover the entire flake. PEEM images in Fig. 3.4(a-c) depict this growth stage. Here, the hBN flake, located to the left of the dashed line, covers about half of the image. The rest of the image corresponds to the SiO_2 substrate. We will refer to the bright areas growing on the hBN flake as pentacene phase D. Diffraction patterns of phase D areas (Fig. 3.5(b)) reveal that they all have the herringbone crystal typical for the standing-up thin film phase of pentacene, similar to growth of pentacene on silicon. [12,17] We have observed pentacene single crystals (in standing-up phase) on hBN flakes with sizes as large as tens of micrometers. Indeed, the diffraction pattern in Fig. 3.5(b) is that of a single crystal within the beam diameter of ~7μm. We have also observed cases where the growth of phase D proceeds in a more branched manner, resulting in a rather polycrystalline film, as evidenced by diffraction. We relate the latter to local substrate contamination.

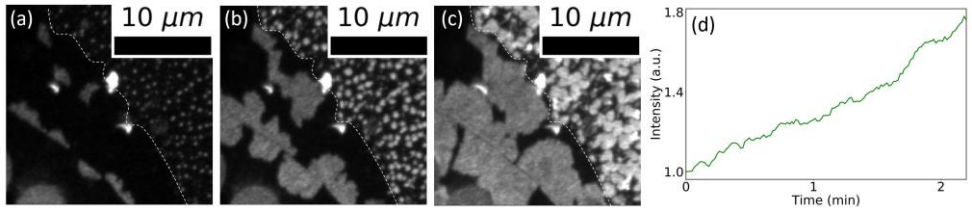

Fig. 3.4 (a-c) PEEM images of growth of pentacene thin film phase on a hBN flake. The flake is located to the left of the dashed line, while to the right of the line is SiO_2. The images show growth of pentacene phase D, which has a higher photoemission intensity than hBN. We also observe nucleation and growth of pentacene on SiO_2 (d) increase in photoemission intensity during formation of phase C before growth of phase D

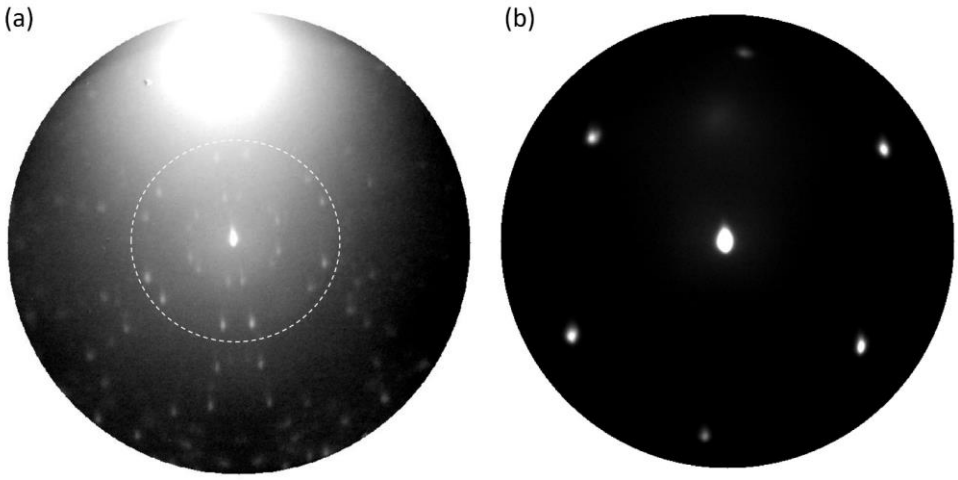

Fig. 3.5 Diffraction patterns of pentacene on hBN flakes. (a) phase C, image intensity is in a log-scale to make higher-order diffraction peaks more visible. The bright circle at the top is due to secondary electrons. The dashed circle encapsulates the lowest-order spots also visible in Fig. 3.2(c) for phase B on graphite. (b) phase D

LEEM-IV spectra of pentacene layers on graphite and hBN:

We used LEEM to also obtain information about the electronic states above the vacuum level for pentacene on graphite and hBN substrates. As mentioned earlier, the energy of the electrons interacting with the sample can be precisely tuned by adjusting the sample potential. The intensity in a real-space LEEM image as well as the intensity of the diffraction spots are functions of incident beam energy. Plotting the intensity of specularly-reflected electrons as a function of beam energy yields a LEEM-IV (intensity vs. voltage) spectrum (referred to above as LEEM reflectivity spectrum). At low electron energies, LEEM-IV spectra are determined mostly by the unoccupied band structure of the sample above the vacuum energy. [28–33] For electron energies at which states are present in the solid and the DOS is high, the incoming electrons have a higher probability of passing into the material, resulting in a lower reflectivity. At energies where the DOS is zero, i.e. at a bandgap, the probability of reflection is higher.

Fig. 3.6 shows LEEM-IV spectra corresponding to pentacene phase B on graphite in black, and the (very similar) phase C on hBN in red. Note that in our experiments, 0 eV corresponds to the vacuum level. At negative energies the incident electrons do not have enough energy to reach the sample, resulting in total reflection. Both spectra show dips at ~1.5 eV and 6 eV.

This figure will be discussed further below along with the pentacene crystal structure in different phases.

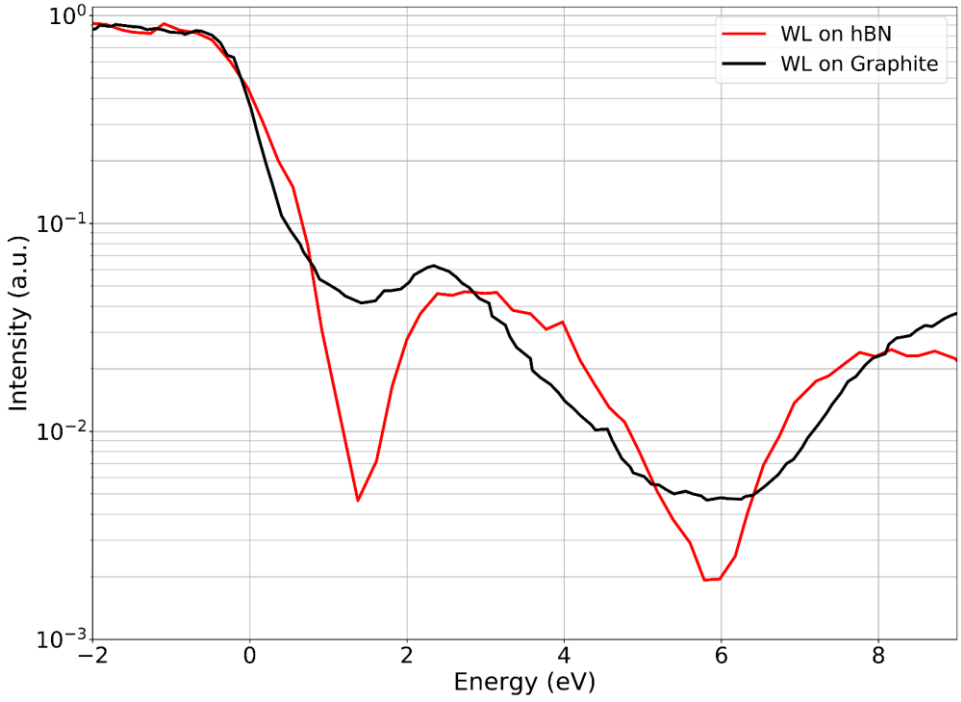

Fig. 3.6 LEEM-IV spectra of pentacene phase B on graphite (black) and phase C on hBN (red)

3.4 Discussion

Now we discuss the structure of pentacene crystals in each of the four phases A-D. First, we focus on phase B (on graphite) and phase C (on hBN). Both of these phases form on flakes in the initial stage of growth, i.e. before formation of phase A (on graphite) and phase D (on hBN), and exhibit striking similarity in their diffraction patterns, see Fig. 3.2(c) and Fig. 3.5(a). Bright-field and dark-field LEEM images of phase B (on graphite) reveal that pentacene forms long narrow crystals in six different orientations on the graphite flake, shown in Fig. 3.3. Similar crystalline domains are expected on hBN flakes due to the similarity of the diffraction images on the graphite and hBN flakes. However, direct imaging with the electron beam on hBN flakes was hampered by charging effects.

To understand the molecular orientation of pentacene in these phases, we need to examine the substrates. Both graphite and hBN have hexagonal crystal lattices, with lattice parameters

very similar to each other and to the molecular carbon frame in pentacene. The C-C distance in pentacene varies between 1.35 Å and 1.45 Å [34,35], while it is 1.42 Å in the basal plane of graphite [34]. The B-N bond length in hBN is 1.446 Å. [36] Phase B of pentacene on graphite has previously been observed, [34,37] with the splitting within each of the six diffraction pairs (as discussed above) reported to be 18±3˚ [34]. Within each crystalline domain the molecules are found to form an oblique lattice with unit cell parameters 17.2±0.5 Å, 7.0±0.5 Å and an angle of 78±3˚. [34] STM, UPS and Penning-ionization electron spectroscopy measurements have found that pentacene molecules in this phase are adsorbed with the molecular plane parallel to the surface. [34,38–40] For pentacene on hBN, the existence of a wetting layer (0.5 nm in thickness) with the same structural features as pentacene adsorbed on graphene, has been reported by Zhang et. al., with DFT calculations showing the phenyl rings of pentacene are oriented parallel to the hBN surface. [5] Park et. al. also reported that the pentacene molecules initially lie flat (with zero tilting angle) parallel to the hBN substrate surface. [23]

Hence, we conclude that phases B (on graphite) and phase C (on hBN) have the same crystal structure, in which the molecules lie flat parallel to the flake surface (planar adsorption geometry), forming a substrate-induced crystal lattice ("templating effect"). We will refer to these phases as the wetting layer (WL). The molecules in the WL form six oblique crystals with two-fold symmetries. In our experiments (Fig. 3.2(c) and Fig. 3.5(a)), the splitting angle within each pair of adjacent diffraction spots is 16.7˚±0.6˚ on graphite (phases B) and 17.7˚±1.3˚ on hBN (phase C), close to the 18±3˚ reported for graphite. [34] Compatible with the lattice mismatch between hBN and graphene, which is ~1.8% [41], the difference in the unit cell parameters of the WL on graphite and hBN in our measurements is also less than 2%.

After formation of the WL, pentacene growth on graphite and hBN proceeds in notably different manners. On graphite, it has been reported that upon further deposition, pentacene forms islands with lateral extensions of several micrometers in which the molecules have a tilted recumbent orientation (28˚-32˚ around their long axis) and crystallize in the Siegrist bulk-phase. [34] Regions with the same diffraction as observed for phase A and dimensions of several micrometers, surrounded by the WL, have also been reported elsewhere, attributed to a bulk phase with tilted recumbent molecules. [37] Hence, we identify phase A as a recumbent bulk crystal phase that grows in islands.

Regarding the growth of pentacene on hBN, literature shows some discrepancies. Similar to our observation of phase D, Zhang et. al. have reported the growth of a standing-up thin-film phase after the WL. [5] In contrast, Amsterdam et. al. did not observe pentacene growth in

the thin film phase and found pentacene to have a recumbent "face-on" orientation (similar to phase A) on top of the initial flat-lying molecules. [24] Park et. al. claimed a flat-lying orientation for the first layer, which gradually transitions with increased pentacene layer thickness to a recumbent phase similar to phase A and eventually standing-up orientation (for thicknesses of tens of nanometers). [23] We did not observe such a gradual transition in our experiments, evidenced by the sudden change of diffraction, and the absence of any intermediate diffraction pattern. Finally, Günder et. al. found pentacene deposited on "single crystal" hBN to have recumbent single-crystals similar to the case of pentacene on graphite (phase A), while on hBN "exfoliated flakes" they found pentacene to form elongated tall fibers with recumbent pentacene in addition to thin film phase covering the areas in between the fibers. [25]

To understand the underlying reasons for the different phases observed in our study, we will briefly discuss the factors affecting the structure of an adsorbed molecular layer. The structure of the adsorbed layer is governed by the energetic competition between the strength of the interactions between the molecule and the substrate on the one hand, and between the molecules on the other hand. One factor affecting this competition is the lattice structure of the substrate surface and the possibility of epitaxial layer growth and templating effect. Both graphite and hBN have a hexagonal lattice structure, similar to the molecular frame of pentacene itself, allowing for the possibility of templating effect. This leads to the formation of the WL on both substrates. A second important factor is the density of states (DOS) of the substrate near the Fermi energy. If the van der Waals interactions between the molecules are stronger than their interaction with the substrate, a standing-up orientation for the molecules is expected. This is more likely for the case of a low electron density at the substrate surface, whereas for higher substrate DOS, the molecules may tend to adopt a lying-down orientation. [19] This dependence was clearly demonstrated in a study of pentacene molecules on a Si(111)-(5×2)Au substrate surface, where addition of 0.5 monolayers of Au turned the substrate into a metallic Si(111)-($\sqrt{3}\times\sqrt{3}$)Au surface and changed the pentacene orientation from standing-up to flat-lying. [19] Growth studies of pentacene molecules on various metal substrates such as Ag(110), Au(111) and Cu(110) have also reported a recumbent orientation for the molecules, [14,20–22] while on semiconducting or insulating surfaces such as Si, SiO_2, organically-terminated Si, Al_2O_3, as well as the semi-metallic Bi(001), pentacene molecules tend to stand up. [12,17–19]

The roughness of the substrate surface, in the form of adsorbates or a damaged crystalline structure, is shown to be another factor affecting growth via local disruption of molecule-substrate interactions. Examples in the literature include observation of a standing-up pentacene phase in place of a recumbent orientation due to sputtering of HOPG with

Ar^+-ions [34], PMMA residue on graphene films. [42] defective MoS_2 substrates [43], and amorphous carbon substrate [44]. On hBN, Günder et. al. have reported only standing-up molecules on defective substrate surfaces with no evidence of any regions with a recumbent orientation [25]. In contrast, we repeatedly observe the formation of the crystalline flat-lying WL on hBN prior to the growth of the standing-up phase, suggesting that the hBN surface condition is such that the molecule-substrate interactions are not disrupted, leading to the observation of templating effect.

We propose that it is the difference in the strength of electronic interactions between pentacene and the substrate that is responsible for the observation of a tilted recumbent phase (phase A) on graphite, versus a standing-up phase (phase D) on hBN. To substantiate that, we refer to Figure 3.6. The two spectra of the WL, which has the same crystal structure on both substrates, exhibit dips at the same energies. However, the minima are strongly broadened on graphite. This indicates significant electronic interaction (hybridization) of the WL pentacene electron states with graphite bands. The sharp minima seen for the hBN substrate suggest very little hybridization between pentacene and hBN, i.e. we are observing a more "pure" spectrum of the WL pentacene in this case. This implies a relatively small interaction energy for the flat-lying molecules on hBN, as compared to the graphite case. Consequently, a standing-up orientation, with energy gain due to intermolecular hybridization, is expected to be more favorable for hBN than for graphite substrates. This reasoning is consistent with our observations: standing-up thin film phase growth of pentacene on hBN flakes vs. recumbent phase growth on graphite. Still we note that on both graphite and hBN, the templating effect is strong enough for the first molecules arriving on the surface to form a flat-lying WL.

3.5 Conclusions

We have studied the growth of pentacene layers on graphite and hBN flakes in real-time, using low-energy electrons as well as UV photons. The two substrates both possess a hexagonal lattice structure with similar unit cell parameters, approximately matching the molecular frame of pentacene. However, they are very different in their electronic properties. We found pentacene to initially form a flat-lying crystalline wetting layer on both substrates. The diffraction patterns corresponding to this wetting layer are strikingly similar for the two substrates. They imply the existence of six oblique crystals with two-fold symmetries, rotated with respect to each other. This crystal lattice is a result of the substrate templating effect.

Upon further sublimation on graphite, we find pentacene to form crystalline islands nucleating and growing from flake edges, in which the molecules adopt a tilted recumbent orientation. On hBN, we observe pentacene to adopt the standing-up thin film phase configuration, contrasting several previous publications. In some literature reports, the appearance of the standing-up phase is observed on intentionally-roughened (or dirty) substrates and hence said to be a result of disrupted molecule-substrate interactions. This explanation cannot be straightforwardly applied here, because prior to the formation of the standing-up phase on hBN, we repeatedly observe the formation of a crystalline wetting-layer with a substrate-induced crystal structure, hinting at undiminished molecule-substrate interactions.

A different and more fundamental explanation for the standing-up thin film phase on hBN as opposed to the tilted recumbent phase seen on graphite is related to the strength of electronic interactions between pentacene molecules and the substrates. LEEM-IV spectra of the wetting layer on both substrates, related to the unoccupied DOS above the vacuum level, indicate a stronger interaction (hybridization) between pentacene and graphite, as compared to pentacene and hBN. We argue that a strong interaction with the substrate makes the recumbent orientation more energetically favourable, explaining the case of graphite. Vice versa, when molecule-molecule interactions are stronger than molecule-substrate interactions, a standing-up orientation is expected, explaining the case of hBN. The differences between the pentacene crystalline structures on the two substrates confirm the possibility of engineered electronic properties by an appropriate choice of the substrate. Our results also illustrate the multi-faceted way the different factors such as density of states of the surface, templating due to surface lattice structure and cleanliness of the surface determine the growth of molecular layers on top.

References

[1] D. Jariwala, S. L. Howell, K. S. Chen, J. Kang, V. K. Sangwan, S. A. Filippone, R. Turrisi, T. J. Marks, L. J. Lauhon, and M. C. Hersam, *Hybrid, Gate-Tunable, van der Waals p-n Heterojunctions from Pentacene and MoS_2*, Nano Lett. **16**, 497 (2016).

[2] S. B. Homan, V. K. Sangwan, I. Balla, H. Bergeron, E. A. Weiss, and M. C. Hersam, *Ultrafast Exciton Dissociation and Long-Lived Charge Separation in a Photovoltaic Pentacene-MoS_2 van der Waals Heterojunction*, Nano Lett. **17**, 164 (2017).

[3] C. Ojeda-Aristizabal, W. Bao, and M. S. Fuhrer, *Thin-Film Barristor: A Gate-Tunable Vertical Graphene-Pentacene Device*, Phys. Rev. B **88**, 035435 (2013).

[4] T. O. Wehling, K. S. Novoselov, S. V. Morozov, E. E. Vdovin, M. I. Katsnelson, A. K. Geim, and A. I. Lichtenstein, *Molecular Doping of Graphene*, Nano Lett. **8**, 173 (2008).

[5] Y. Zhang et al., *Probing Carrier Transport and Structure-Property Relationship of Highly Ordered Organic Semiconductors at the Two-Dimensional Limit*, Phys. Rev. Lett. **116**, 016602 (2016).

[6] D. He et al., *Two-Dimensional Quasi-Freestanding Molecular Crystals for High-Performance Organic Field-Effect Transistors*, Nat Commun **5**, 5162 (2014).

[7] C. H. Lee et al., *Epitaxial Growth of Molecular Crystals on van der Waals Substrates for High-Performance Organic Electronics*, Adv. Mater. **26**, 2812 (2014).

[8] Y. Kato, S. Iba, R. Teramoto, T. Sekitani, T. Someya, H. Kawaguchi, and T. Sakurai, *High Mobility of Pentacene Field-Effect Transistors with Polyimide Gate Dielectric Layers*, Appl. Phys. Lett. **84**, 3789 (2004).

[9] H. Klauk, M. Halik, U. Zschieschang, G. Schmid, W. Radlik, and W. Weber, *High-Mobility Polymer Gate Dielectric Pentacene Thin Film Transistors*, J. Appl. Phys. **92**, 5259 (2002).

[10] O. D. Jurchescu, J. Baas, and T. T. M. Palstra, *Effect of Impurities on the Mobility of Single Crystal Pentacene*, Appl. Phys. Lett. **84**, 3061 (2004).

[11] J. Y. Lee, S. Roth, and Y. W. Park, *Anisotropic Field Effect Mobility in Single Crystal Pentacene*, Appl. Phys. Lett. **88**, 252106 (2006).

[12] FJ. Meyer zu Heringdorf, M. C. Reuter, and & R. M. Tromp, *Growth Dynamics of Pentacene Thin Films*, Nature **412**, 517 (2001).

[13] C. B. France, P. G. Schroeder, and B. A. Parkinson, *Direct Observation of a Widely Spaced Periodic Row Structure at the Pentacene/Au(111) Interface Using Scanning Tunneling Microscopy*, Nano Lett **2**, 693 (2002).

[14] Y. L. Wang, W. Ji, D. X. Shi, S. X. Du, C. Seidel, Y. G. Ma, H. J. Gao, L. F. Chi, and H. Fuchs, *Structural Evolution of Pentacene on a Ag(110) Surface*, Phys. Rev. B **69**, 075408 (2004).

[15] L. Casalis, M. F. Danisman, B. Nickel, G. Bracco, T. Toccoli, S. Iannotta, and G. Scoles, *Hyperthermal Molecular Beam Deposition of Highly Ordered Organic Thin Films*, Phys. Rev. Lett. **90**, 206101 (2003).

[16] S. Lukas, S. Söhnchen, G. Witte, and C. Wöll, *Epitaxial Growth of Pentacene Films on Metal Surfaces*, ChemPhysChem **5**, 266 (2004).

[17] A. Al-Mahboob, J. T. Sadowski, Y. Fujikawa, K. Nakajima, and T. Sakurai, *Kinetics-Driven Anisotropic Growth of Pentacene Thin Films*, Phys. Rev. B **77**, 035426 (2008).

[18] F. J. Meyer Zu Heringdorf, M. C. Reuter, and R. M. Tromp, *The Nucleation of Pentacene Thin Films*, Appl. Phys. A **78**, 787 (2004).

[19] G. E. Thayer, J. T. Sadowski, F. Meyer Zu Heringdorf, T. Sakurai, and R. M. Tromp, *Role of Surface Electronic Structure in Thin Film Molecular Ordering*, Phys. Rev. Lett. **95**, 256106 (2005).

[20] J. H. Kang and X. Y. Zhu, *Pi-Stacked Pentacene Thin Films Grown on Au(111)*, Appl. Phys. Lett. **82**, 3248 (2003).

[21] P. G. Schroeder, C. B. France, J. B. Park, and B. A. Parkinson, *Energy Level Alignment and Two-Dimensional Structure of Pentacene on Au(111) Surfaces*, J. Appl. Phys. **91**, 3010 (2002).

[22] S. Lukas, G. Witte, and C. Wöll, *Novel Mechanism for Molecular Self-Assembly on Metal Substrates: Unidirectional Rows of Pentacene on Cu(110) Produced by a Substrate-Mediated Repulsion*, Phys. Rev. Lett. **88**, 028301 (2002).

[23] B. Park et al., *Anomalous Ambipolar Transport of Organic Semiconducting Crystals via Control of Molecular Packing Structures*, ACS Appl. Mater. Interfaces **9**, 27839 (2017).

[24] S. H. Amsterdam et al., *Tailoring the Optical Response of Pentacene Thin Films via Templated Growth on Hexagonal Boron Nitride*, J. Phys. Chem. Lett **12**, 26 (2021).

[25] D. Gunder, K. Watanabe, T. Taniguchi, and G. Witte, *Van der Waals Bound Organic/2D Insulator Hybrid Structures: Epitaxial Growth of Acene Films on hBN(001) and the Influence of Surface Defects*, ACS Appl. Mater. Interfaces **12**, 38757 (2020).

[26] S. M. Schramm, J. Kautz, A. Berghaus, O. Schaff, R. M. Tromp, and S. J. van der Molen, *Low-Energy Electron Microscopy and Spectroscopy with ESCHER: Status and Prospects*, IBM J. Res. & Dev. **55**, 1:1 (2011).

[27] R. M. Tromp, J. B. Hannon, A. W. Ellis, W. Wan, A. Berghaus, and O. Schaff, *A New Aberration-Corrected, Energy-Filtered LEEM/PEEM Instrument. I. Principles and Design*, Ultramicroscopy **110**, 852 (2010).

[28] J. Jobst, J. Kautz, D. Geelen, R. M. Tromp, and S. J. van der Molen, *Nanoscale Measurements of Unoccupied Band Dispersion in Few-Layer Graphene*, Nat. Commun. **6**, 8926 (2015).

[29] J. Jobst, A. J. H. van der Torren, E. E. Krasovskii, J. Balgley, C. R. Dean, R. M. Tromp, and S. J. van der Molen, *Quantifying Electronic Band Interactions in van der Waals Materials Using Angle-Resolved Reflected-Electron Spectroscopy*, Nat. Commun. **7**, 13621 (2016).

[30] J. B. Pendry, *Theory of Photoemission*, Surf. Sci. **57**, 679 (1976).

[31] J. B. Pendry, *The Application of Pseudopotentials to Low-Energyelectron Diffraction II: Calculation of the Reflectedintensities*, J. Phys. C: Solid State Phys. **2**, 2273 (1969).

[32] V. N. Strocov, E. E. Krasovskii, W. Schattke, N. Barrett, H. Berger, D. Schrupp, and R. Claessen, *Three-Dimensional Band Structure of Layered $TiTe_2$: Photoemission Final-State Effects*, Phys. Rev. B. **74**, 195125 (2006).

[33] V. N. Strocov, H. I. Starnberg, and P. O. Nilsson, *Mapping the Excited-State Bands above the Vacuum Level with VLEED: Principles, Results for Cu, and the Connection to Photoemission*, J. Phys.: Condens. Matter **8**, 7539 (1996).

[34] J. Götzen, D. Käfer, C. Wöll, and G. Witte, *Growth and Structure of Pentacene Films on Graphite: Weak Adhesion as a Key for Epitaxial Film Growth*, Phys. Rev. B **81**, 085440 (2010).

[35] R. B. Campbell, J. Monteath Robertson, and J. Trotter, *The Crystal and Molecular Structure of Pentacene*, Acta. Cryst. **14**, 705 (1961).

[36] O. Hod, *Graphite and Hexagonal Boron-Nitride Have the Same Interlayer Distance. Why?*, J. Chem. Theory Comput. **8**, 1360 (2012).

[37] H. W. Liu, A. Al-Mahboob, Y. Fujikawa, N. Fukui, T. Hitosugi, T. Hashizume, Q. K. Xue, and T. Sakurai, *Pentacene Growth on Graphite Investigated by Low-Energy Electron Microscope*, J. Cryst. Growth **312**, 967 (2010).

[38] Y. Harada, H. Ozaki, and K. Ohno, *Selective Observation of Outermost Surface Layer during Epitaxial Growth by Penning-Ionization Electron Spectroscopy: Pentacene on Grayhite*, Phys. Rev. Lett. **52**, 2269 (1984).

[39] H. Fukagawa, H. Yamane, T. Kataoka, S. Kera, M. Nakamura, K. Kudo, and N. Ueno, *Origin of the Highest Occupied Band Position in Pentacene Films from Ultraviolet Photoelectron Spectroscopy: Hole Stabilization versus Band Dispersion*, Phys. Rev. B. **73**, 245310 (2006).

[40] W. Chen, H. Huang, A. Thye, and S. Wee, *Molecular Orientation Transition of Organic Thin Films on Graphite: The Effect of Intermolecular Electrostatic and Interfacial Dispersion Forces*, Chem. Commun., 4276 (2008).

[41] G. Giovannetti, P. A. Khomyakov, G. Brocks, P. J. Kelly, and J. Van Den Brink, *Substrate-Induced Band Gap in Graphene on Hexagonal Boron Nitride: Ab Initio Density Functional Calculations*, Phys. Rev. B **76**, 073103 (2007).

[42] W. H. Lee, J. Park, S. H. Sim, S. Lim, K. S. Kim, B. H. Hong, and K. Cho, *Surface-Directed Molecular Assembly of Pentacene on Monolayer Graphene for High-Performance Organic Transistors*, J. Am. Chem. Soc. **133**, 4447 (2011).

[43] T. Breuer, T. Maßmeyer, A. Mänz, S. Zoerb, B. Harbrecht, and G. Witte, *Structure of van der Waals Bound Hybrids of Organic Semiconductors and Transition Metal*

Dichalcogenides: The Case of Acene Films on MoS_2, Phys. Status Solidi RRL **10**, 905 (2016).

[44] K. Kim, E. J. G. Santos, T. H. Lee, Y. Nishi, and Z. Bao, *Epitaxially Grown Strained Pentacene Thin Film on Graphene Membrane*, Small **11**, 2037 (2015).

Supporting Information

Desorption of pentacene from graphite by heating and repeat of the growth experiment

The sequence of LEEM images in Fig. S3.1 shows the desorption process of the pentacene layers from the graphite surface of Fig. 3.1 as a result of heating of the sample up to a temperature of 600˚C. Fig. S3.1(a), resembling Fig. 3.2(a), shows the two different phases of pentacene on graphite. Note that the pentacene area at the bottom left of the image (phase A) is desorbed completely before the pentacene elsewhere on the sample (phase B) shows any change at all. This shows the interaction between the pentacene molecules and graphite is stronger than between the pentacene molecules in phase A. After the desorption of pentacene, the sample was cooled down and the sublimation of pentacene (from the Knudsen cell) on graphite was repeated. Prior to re-sublimation, diffraction patterns on the flake did not contain any features from pentacene, while real-space images in some areas showed non-homogeneity and possible remnants from the previous sublimation round, as well as electron beam imprints (see Fig. S3.2), indicating that the heating of the sample did not completely clean the surface of the entire flake. The new sublimation of pentacene on the graphite flake proceeded mostly the same as the previous round showing the same developments as shown in Fig. 3.1. However, this time, also regions with high photoemission intensity appeared on the flake, similar to those which had appeared on the substrate, as can be seen in Fig. S3.3(a). As expected, the diffraction pattern corresponding to these regions, shown in Fig. S3.3(b), is the same as observed for standing-up thin film pentacene phase.

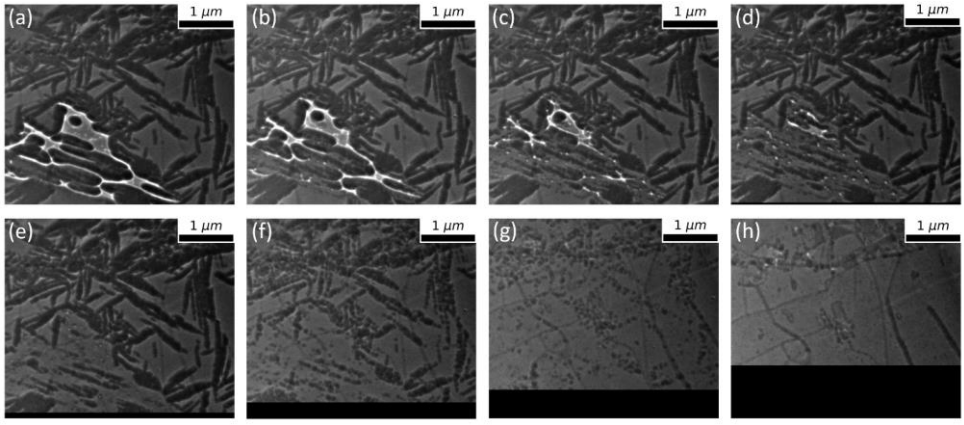

Fig. S3.1 Gradual desorption of pentacene from a graphite flake as a result of heating. Note that before the bright feature at the bottom left (phase A) has evaporated, no change at all can be seen on the rest of the surface (phase B)

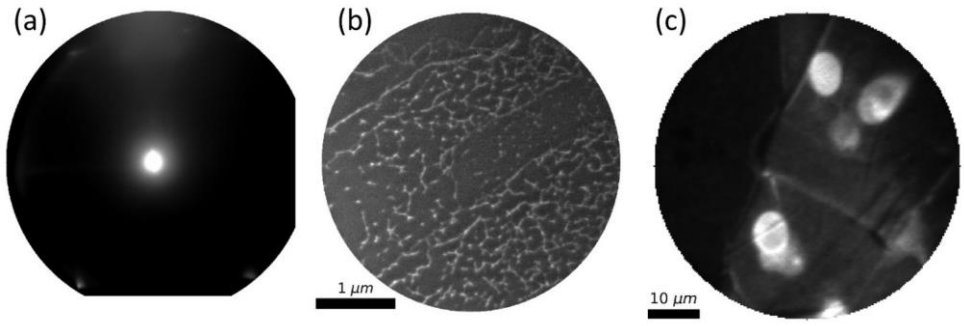

Fig. S3.2 Images of the graphite flake after heating and desorption of pentacene (a) diffraction pattern showing diffraction spots of graphite with no trace of the pentacene crystal diffraction patterns shown in Fig. 3.2(b-c) (b) Real-space image showing features on the surface of the flake, possible remnants from the previous sublimation round (c) beam imprints in a PEEM image

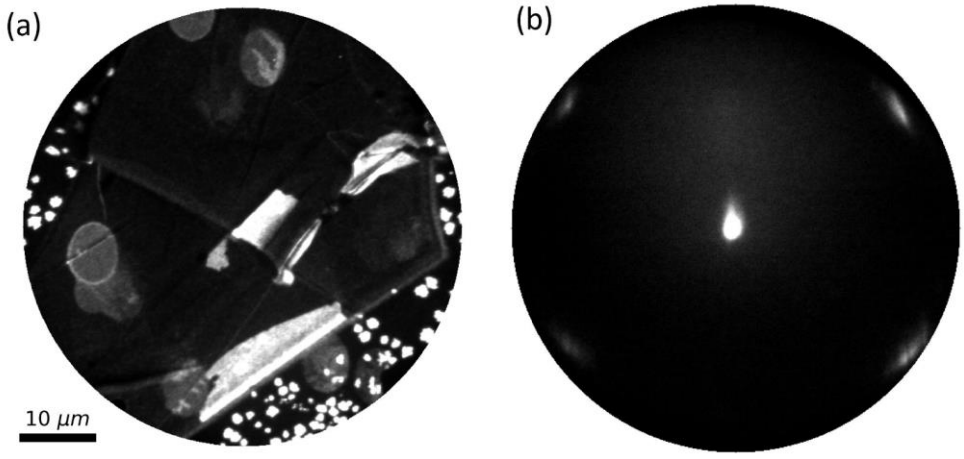

Fig. S3.3 Re-sublimation of pentacene on the same graphite flake. (a) PEEM image showing regions of very high intensity on the flake (b) The diffraction pattern corresponding to such regions